Journal of Sound and Vibration (2000) **229**(3), 695–707
doi:10.1006/jsvi.1999.2511, available online at http://www.idealibrary.com on IDEAL®

CURVE SQUEAL OF TRAIN WHEELS, PART 2: WHICH WHEEL MODES ARE PRONE TO SQUEAL?

MARIA A. HECKL

Department of Mathematics, Keele University, Keele, Staffordshire ST5 5BG, England

(*Received* 25 *August* 1998, *and in final form* 5 *August* 1999)

This paper presents a frequency-domain analysis of a friction-driven wheel that is responsible for wheel squeal. A linear friction characteristic is assumed. The wheel motion is written as a superposition of bending modes. The modal properties (damping, frequency, impulse response amplitude of each mode) of the free wheel are known; the equivalent properties of the friction-driven wheel are calculated from complicated sets of linear and non-linear equations derived from the governing equation, which is an integrodifferential equation for the wheel displacement. An approximate analytical criterion is obtained, which allows one to predict easily whether a mode with given free-wheel properties is prone to squeal. The influence of features of the friction characteristic is also revealed. Precise numerical simulations give the growth rates, frequencies and complex amplitudes of the friction-driven wheel. These properties can be combined to give the time history of the wheel velocity. Time histories obtained in this way are compared with those obtained from direct evaluation of the governing equation in the time domain. Such comparison provides a reliable test of the time- and frequency-domain analysis.

1. INTRODUCTION

Curve squeal of trains is generated if a train traversing a bend performs a crabbing motion with its wheels because they cannot align themselves tangentially to the rail. As a consequence of this crabbing motion, a dry friction force acts on the wheels in the lateral direction. The friction force excites bending oscillations of the wheels, and they radiate sound into the surrounding air.

The frequency spectrum of an individual squealing wheel contains one (or a few) very sharp peaks. Each peak corresponds to the resonance of a certain bending mode of the wheel. The resonance is self-excited, i.e. the dry friction force that drives the wheel motion is itself dependent on the wheel motion. The functional dependence between friction force and wheel velocity (called the friction characteristic) is an essential feature for the generation of squeal noise. For example, a linear friction characteristic, where the friction force rises with the wheel velocity, represents a force with negative damping, and it is intuitively obvious, that this would lead to an oscillation with growing amplitude.

Wheel squeal is associated with the stick/slip mechanism, where the friction force oscillates in rapid succession between rolling friction and sliding friction. This is

0022-460X/00/030695 + 13 $35.00/0

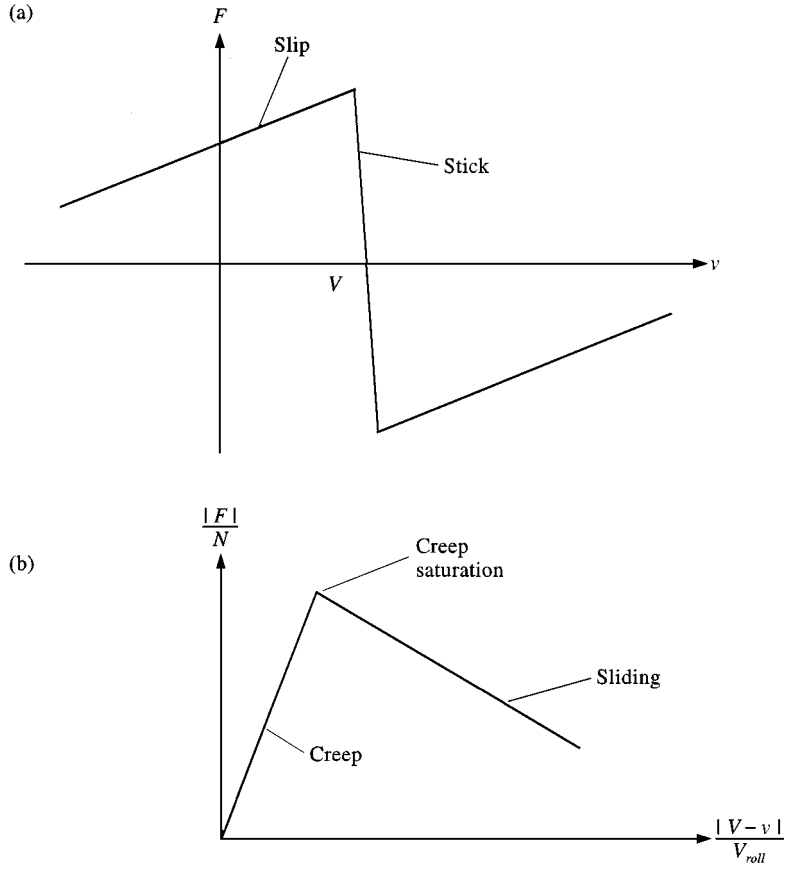

Figure 1. (a) Friction characteristic (F: friction force, v: wheel velocity at the contact point, V: crabbing speed). (b) Corresponding creep curve (F, v, V as in (a), N: normal load, V_{roll}: rolling velocity).

described by the friction characteristic shown in Figure 1(a). The slip and the stick section of the friction characteristic play two different roles. At low velocity amplitudes (below the crabbing speed) the oscillation is slip-only, traversing only the linear part of the friction characteristic. This linear excitation is responsible for the instability of some wheel modes and drives them to grow exponentially. Once the velocity amplitude reaches the crabbing speed, the oscillation becomes stick/slip, and the excitation is now non-linear. The sticking is responsible for the limitation of the amplitude, leading to a limit-cycle oscillation.

In the railway community, the friction force is conventionally specified in terms of a creep curve (see, for example, references [1, 2]), which gives the traction coefficient (ratio between friction force and normal load) as a function of creep (ratio between relative velocity and rolling velocity). The creep curve that is equivalent to our form of the friction characteristic, is shown in Figure 1(b). It shows the magnitudes of the friction force (scaled with normal load N) and the relative velocity (scaled with the rolling velocity V_{roll}). The creep and the sliding

section of this curve correspond respectively to the stick and slip section of Figure 1(a). The feature that induces instability is the positive slope of the slip section in Figure 1(a) and, correspondingly, the negative slope of the sliding section in Figure 1(b).

When tapped with a force perpendicular to its plane, a wheel oscillates with a superposition of many modes with shapes described by mode numbers (m, n), where m is the number of nodal lines and n is the number of nodal circles. Not all modes of a given wheel are affected by the phenomenon of self-excitation due to the dry friction force; in fact only a small number of modes, often just a single mode, are selected for resonance excitation by the dry friction force. In experiments with a small-scale rig, simulating wheel crabbing with several different model wheels, we found that some wheels squealed with mode $(2, 1)$, while other wheels with similar geometry and material squealed with mode $(3, 1)$ or not at all. Figure 2 shows measured spectra for one such wheel. If the wheel is tapped, it responds with a spectrum featuring modes $(2, 1)$ and $(3, 1)$ (see Figure 2(a)). Only mode $(3, 1)$ appears in the spectrum of the squeal produced by that wheel (see Figure 2(b)).

Although curve squeal has been much investigated theoretically and experimentally [2–7], it is still unclear why some wheel modes squeal, but not others. This gap in knowledge has been pointed out in a state-of-the-art article by Remington [1]. The aim of this paper is to predict which modes are squeal-prone, depending on the wheel's properties (in particular its modal parameters) and on features of the friction characteristic. We consider a wheel with several modes, which are all simultaneously subjected to the dry friction force. This represents an extension of the work by Rudd [4], who considered the case where the friction force acts on an isolated wheel mode described by its modal mass and modal stiffness. The mathematical details of our model are described in an earlier paper [7]. In the present paper, the focus is on the wheel modes and results are therefore obtained in the frequency domain. These results also complement the time-domain results reported in the earlier paper.

We distinguish between squeal-prone modes and squealing modes. The term "squeal-prone mode" (or unstable mode) applies to exponentially growing, slip-only, oscillations and a linear friction characteristic. The term "squealing mode" applies to stick/slip limit-cycle oscillations and a non-linear friction characteristic. Some, but not necessarily all, squeal-prone modes are squealing modes. The distinction between squeal-prone and squealing modes does not matter in the many cases where there is one squeal-prone mode; this mode is always a squealing mode.

A general description of the mathematical model for curve squeal is given in Section 2. The governing equation is a linear integrodifferential equation for the wheel displacement. Its complex eigenfrequencies and corresponding displacement amplitudes are calculated in Section 3. Also given in this section is a simple analytical criterion as to whether or not a mode is squeal-prone. Predictions from numerical simulations are presented in Section 4, and compared with the results from the time-history calculations of Heckl and Abrahams [7].

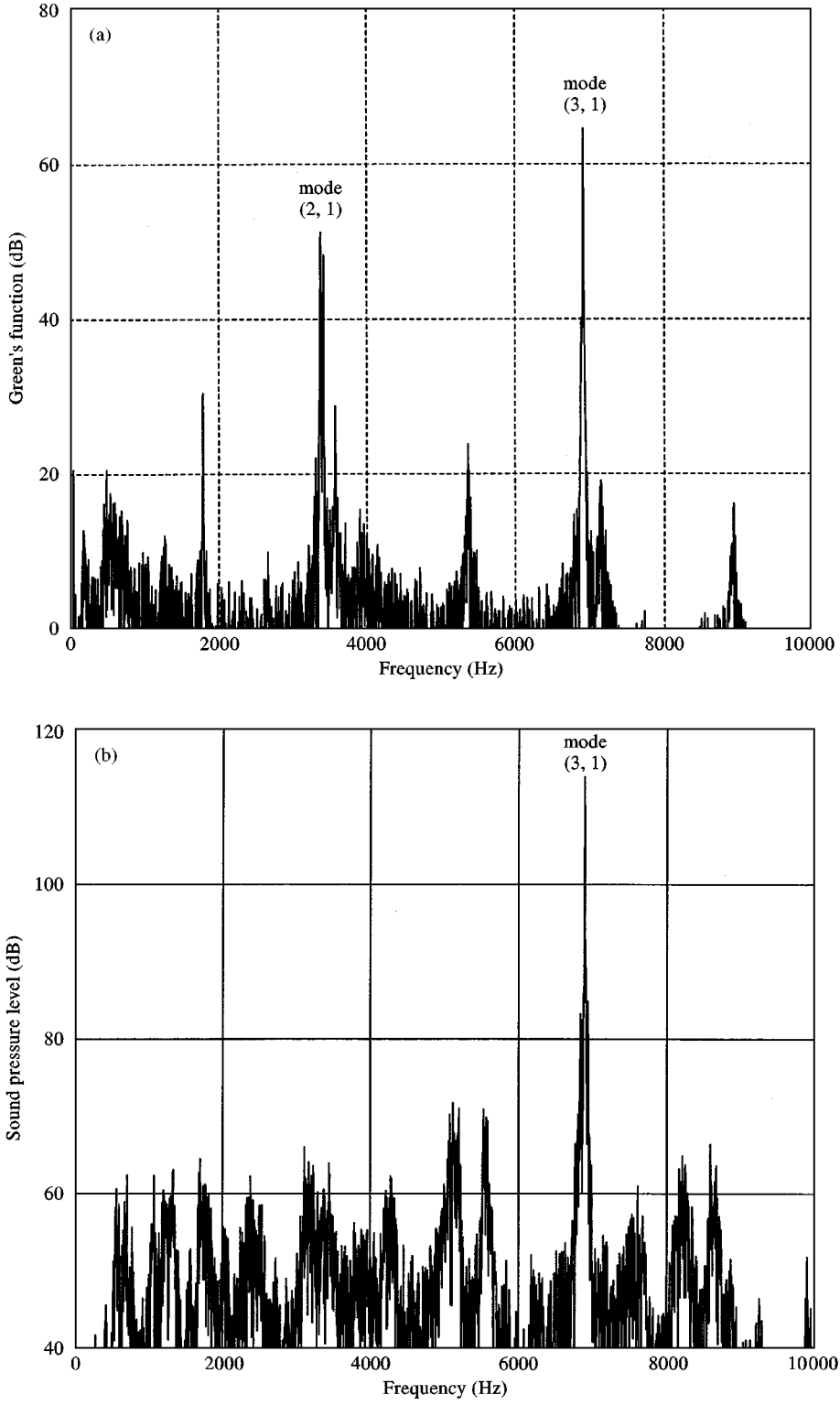

Figure 2. Frequency spectra of a model wheel: (a) tapped wheel; (b) squealing wheel.

2. GENERAL FORMULATION OF THE MATHEMATICAL MODEL

The governing equation for the transverse displacement w of a friction-driven wheel is given by (see reference [7])

$$w(r, \varphi, t) = \int_{t'=0}^{t} F(v(r_f, \varphi_f, t'))G(r, \varphi; r_f, \varphi_f; t - t')\,\mathrm{d}t'. \tag{2.1}$$

(r, φ) is an observer point on the wheel and (r_f, φ_f) is the contact point with the rail where the friction force acts. F is the friction force; its dependence on the wheel velocity v at the contact point is described by the friction characteristic $F(v)$. G, the Green's function, is the displacement response of the free wheel to an impulse force acting at point (r_f, φ_f).

The friction characteristic $F(v)$ describes the feedback between the wheel oscillation and the friction force driving this oscillation. We assume that $F(v)$ is a linear function,

$$F(v) = F_0 + \gamma v. \tag{2.2}$$

γ denotes the (positive) slope of the curve; it can be seen as a "negative damping coefficient" associated with the friction force. F_0 is the mean part of the friction force. This friction characteristic describes a slip-only motion; it is valid for small velocity amplitudes and allows exponential amplitude growth.

The Green's function characterizes the *free* wheel, i.e., the wheel that is merely held by the axle without making contact with the rail. It is a superposition of bending modes of the wheel,

$$G(r, \varphi; r_f, \varphi_f: t - t') = \begin{cases} \text{real} \displaystyle\sum_{m=0}^{\infty} \sum_{n=1}^{\infty} g_{mn}(r, \varphi; r_f, \varphi_f)\mathrm{e}^{-\mathrm{i}(\omega_{mn} + \mathrm{i}\delta_{mn})(t-t')} & \text{for } t \geqslant t', \\ 0 & \text{for } t < t'. \end{cases} \tag{2.3a, b}$$

ω_{mn}, δ_{mn} and g_{mn} are respectively the frequency, growth rate and amplitude of mode (m, n). These Green's function components can be determined experimentally by exciting the free wheel with an impulse point force and then measuring the time history of the resulting motion. The frequency, growth rate and amplitude of each mode are then inferred from the measured time history. The growth rates δ_{mn} of all modes are negative, describing an oscillation decay; any relevant damping mechanisms (such as radiation losses and various forms of internal damping) are included in the measured δ_{mn} values. This experimental approach is possible for wheels of any geometry. For wheels of simple geometries, the frequencies and amplitudes of the Green's function can be calculated theoretically (see reference [7]). The growth rates would have to be estimated from the loss factor of the wheel material.

It is convenient to combine ω_{mn} and δ_{mn} to define the complex eigenfrequency

$$\psi_{mn} = \omega_{mn} + \mathrm{i}\delta_{mn}. \tag{2.4}$$

An integrodifferential equation can be obtained for the wheel displacement $w(r_f, \varphi_f, t)$ from equation (2.1) by evaluating this equation at point (r_f, φ_f), and using the linear friction characteristic (2.2) with the substitution $v = \dot{w}$. Mathematically speaking (see for example reference [8, section 3.1.3]), this integrodifferential equation for w is of the Volterra type (variable upper integration limit) of the second kind (unknown function w inside and outside the integrand). Its kernel is the Green's function, which is a difference kernel because its time dependence is a function of only $t - t'$. It is non-homogeneous due to the constant term F_0.

The standard method of solving this type of equation is by use of the Laplace transform (see, for example, reference [9, pp. 972–973]). This method involves integration in the complex plane and does not focus particularly on complex eigenfrequencies. We take a different, but equivalent, approach, which is modelled on the modal nature of the wheel and designed to give explicitly the complex eigenfrequencies of the friction-driven wheel.

3. COMPLEX EIGENFREQUENCIES OF THE FRICTION-DRIVEN WHEEL

We distinguish between the complex eigenfrequencies of the free wheel and those of the friction-driven wheel. For the free wheel, they are known and defined by equation (2.4). For the friction-driven wheel, they are unknown; by analogy to the notation for the free wheel, they are denoted by Ψ_{mn} and defined by

$$\Psi_{mn} = \Omega_{mn} + \mathrm{i}\Delta_{mn}, \tag{3.1}$$

where Ω_{mn} and Δ_{mn} are respectively the frequency and growth rate of mode (m, n) of the friction-driven wheel. The sign of Δ_{mn} indicates the stability behaviour of mode (m, n): if $\Delta_{mn} > 0$, the mode is unstable, and if $\Delta_{mn} \leqslant 0$, the mode is stable.

We restrict our considerations to a wheel with a finite number of modes,

$$m = 0, \ldots, M, \qquad n = 1, \ldots, N. \tag{3.2}$$

The displacement $w(r_f, \varphi_f, t)$ of the friction-driven wheel can then be written as a superposition of modes,

$$w(r_f, \varphi_f, t) = \tfrac{1}{2}\left[w_0 + w_0^* + \sum_{m=0}^{M} \sum_{n=1}^{N} (w_{mn} \mathrm{e}^{-\mathrm{i}\Psi_{mn} t} + w_{mn}^* \mathrm{e}^{\mathrm{i}\Psi_{mn}^* t}) \right]. \tag{3.3}$$

To allow the subsequent manipulations, the real part of the complex term has been expressed as half the sum of the complex term and its complex conjugate. Equation (3.3) is the equivalent of the free-wheel equation (2.3a). The w_{mn} are the

(complex) displacement amplitudes; they are unknown and correspond to the amplitudes g_{mn}, which are known. The constant term w_0, which is also unknown, has been introduced because the friction force has a constant term F_0.

The time derivative of equation (3.3) gives the velocity of the friction-driven wheel,

$$v(r_f, \varphi_f, t) = \tfrac{1}{2} \sum_{m=0}^{M} \sum_{n=1}^{N} (- \mathrm{i}\Psi_{mn} w_{mn} \mathrm{e}^{-\mathrm{i}\Psi_{mn} t} + \mathrm{i}\Psi^*_{mn} w^*_{mn} \mathrm{e}^{\mathrm{i}\Psi^*_{mn} t}). \tag{3.4}$$

If the governing equation (2.1) is evaluated at point (r_f, φ_f), all the time histories in this equation can be substituted for by sums over modes. Expression (3.3) is substituted into the left-hand side of equation (2.1). Substituted into the right-hand side of equation (2.1) are the linear friction characteristic (2.2) with equation (3.4) for the wheel velocity, and the Green's function (2.3a), with its sums truncated. The resulting equation is

$$\begin{aligned} &\tfrac{1}{2}\left[w_0 + w_0^* + \sum_{m=0}^{M} \sum_{n=1}^{N} (w_{mn} \mathrm{e}^{-\mathrm{i}\Psi_{mn} t} + w^*_{mn} \mathrm{e}^{\mathrm{i}\Psi^*_{mn} t}) \right] \\ &\quad = \int_0^t \left[F_0 + \gamma \tfrac{1}{2} \sum_{m=0}^{M} \sum_{n=1}^{N} (-\mathrm{i}\Psi_{mn} w_{mn} \mathrm{e}^{-\mathrm{i}\Psi_{mn} t'} + \mathrm{i}\Psi^*_{mn} w^*_{mn} \mathrm{e}^{\mathrm{i}\Psi^*_{mn} t'}) \right] \cdot \\ &\qquad \cdot \left[\tfrac{1}{2} \sum_{m'=0}^{M} \sum_{n'=1}^{N} (g_{m'n'} \mathrm{e}^{-\mathrm{i}\psi_{m'n'}(t-t')} + g^*_{m'n'} \mathrm{e}^{\mathrm{i}\psi^*_{m'n'}(t-t')}) \right] \mathrm{d}t'. \end{aligned} \tag{3.5}$$

where $g_{m'n'}$ has been used to abbreviate $g_{m'n'}(r_f, \varphi_f; r_f, \varphi_f)$. A number of lengthy but straightforward, manipulations follow, which are not shown here. They include: multiplying out the brackets in the integrand, putting the t-dependent terms outside the integral, performing the integration over the t'-dependent terms to obtain new t-dependent terms, multiplying both sides of the equation by 2, and sorting the terms on the right-hand side into constant terms and terms with factors $\mathrm{e}^{-\mathrm{i}\Psi_{mn} t}$, $\mathrm{e}^{\mathrm{i}\Psi^*_{mn} t}$, $\mathrm{e}^{-\mathrm{i}\psi_{m'n'} t}$, $\mathrm{e}^{\mathrm{i}\psi^*_{m'n'} t}$. The final result is

$$\begin{aligned} &w_0 + w_0^* + \sum_{m=0}^{M} \sum_{n=1}^{N} (w_{mn} \mathrm{e}^{-\mathrm{i}\Psi_{mn} t} + w^*_{mn} \mathrm{e}^{\mathrm{i}\Psi^*_{mn} t}) \\ &\quad = \sum_{m'=0}^{M} \sum_{n'=1}^{N} \left(g_{m'n'} \frac{F_0}{\mathrm{i}\psi_{m'n'}} + g^*_{m'n'} \frac{F_0}{-\mathrm{i}\psi^*_{m'n'}} \right) \\ &\qquad + \sum_{m=0}^{M} \sum_{n=1}^{N} \mathrm{e}^{-\mathrm{i}\Psi_{mn} t} \tfrac{1}{2} \gamma \Psi_{mn} w_{mn} \sum_{m'=0}^{M} \sum_{n'=1}^{N} \left(\frac{g_{m'n'}}{\Psi_{mn} - \psi_{m'n'}} + \frac{g^*_{m'n'}}{\Psi_{mn} + \psi^*_{m'n'}} \right) \\ &\qquad + \sum_{m=0}^{M} \sum_{n=1}^{N} \mathrm{e}^{\mathrm{i}\Psi^*_{mn} t} \tfrac{1}{2} \gamma \Psi^*_{mn} w^*_{mn} \sum_{m'=0}^{M} \sum_{n'=1}^{N} \left(\frac{g_{m'n'}}{\Psi^*_{mn} + \psi_{m'n'}} + \frac{g^*_{m'n'}}{\Psi^*_{mn} - \psi^*_{m'n'}} \right) \end{aligned}$$

$$+\sum_{m'=0}^{M}\sum_{n'=1}^{N} e^{-i\psi_{m'n'}t}\, g_{m'n'}\left[\frac{-F_0}{i\psi_{m'n'}}+\tfrac{1}{2}\gamma\sum_{m=0}^{M}\sum_{n=1}^{N}\left(\frac{\Psi_{mn}w_{mn}}{\psi_{m'n'}-\Psi_{mn}}-\frac{\Psi^*_{mn}w^*_{mn}}{\psi_{m'n'}+\Psi^*_{mn}}\right)\right]$$

$$+\sum_{m'=0}^{M}\sum_{n'=1}^{N} e^{i\psi^*_{m'n'}t}\, g^*_{m'n'}\left[\frac{F_0}{i\psi^*_{m'n'}}-\tfrac{1}{2}\gamma\sum_{m=0}^{M}\sum_{n=1}^{N}\left(\frac{\Psi_{mn}w_{mn}}{\psi^*_{m'n'}+\Psi_{mn}}+\frac{\Psi^*_{mn}w^*_{mn}}{-\psi^*_{m'n'}+\Psi^*_{mn}}\right)\right]. \tag{3.6}$$

This equation is satisfied if the constant terms as well as the coefficients of $e^{-i\Psi_{mn}t}$, $e^{i\Psi^*_{mn}t}$, $e^{-i\psi_{m'n'}t}$ and $ei^{\psi^*_{m'n'}t}$ are equal on either side of the equation.

Equating the constants on either side of the equation gives

$$w_0+w_0^*=F_0\sum_{m'=0}^{M}\sum_{n'=1}^{N}\left(\frac{g_{m'n'}}{i\psi_{m'n'}}-\frac{g^*_{m'n'}}{i\psi^*_{m'n'}}\right). \tag{3.7}$$

This determines the real part of the unknown w_0.

Equating the coefficients of $e^{-i\Psi_{mn}t}$ gives

$$\tfrac{1}{2}\gamma\Psi_{mn}\sum_{m'=0}^{M}\sum_{n'=1}^{N}\left(\frac{g_{m'n'}}{\Psi_{mn}-\psi_{m'n'}}+\frac{g^*_{m'n'}}{\Psi_{mn}+\psi^*_{m'n'}}\right)=1,\quad (m=0,\ldots,M,\ n=1,\ldots,N). \tag{3.8}$$

This is a non-linear equation for the complex eigenfrequencies Ψ_{mn}. It can be converted into a polynomial equation by multiplying both sides of equation (3.8) by the product of all denominators in the sum. The resulting polynomial equation has degree $2MN$, and has thus twice as many solutions as required. The second set of solutions is $-\Psi^*_{mn}$ $(m=0,\ldots,M,\ n=1,\ldots,N)$. Equation (3.8) can thus be seen as the characteristic equation of the governing equation (2.1) with roots Ψ_{mn}, $-\Psi^*_{mn}$ $(m=0,\ldots,M, n=1,\ldots,N)$. Equating the coefficients of $e^{i\Psi^*_{mn}t}$ in equation (3.6) gives the complex conjugate of equation (3.8).

Equating the coefficients of $e^{-i\psi_{m'n'}t}$ and $e^{i\psi^*_{m'n'}t}$ gives respectively

$$\tfrac{1}{2}\gamma\sum_{m=0}^{M}\sum_{n=1}^{N}\left(\frac{\Psi_{mn}w_{mn}}{\psi_{m'n'}-\Psi_{mn}}-\frac{\Psi^*_{mn}w^*_{mn}}{\psi_{m'n'}+\Psi^*_{mn}}\right)=\frac{F_0}{i\psi_{m'n'}} \tag{3.9a}$$

and

$$\tfrac{1}{2}\gamma\sum_{m=0}^{M}\sum_{n=1}^{N}\left(\frac{\Psi_{mn}w_{mn}}{\psi^*_{m'n'}+\Psi_{mn}}+\frac{\Psi^*_{mn}w^*_{mn}}{-\psi^*_{m'n'}+\Psi^*_{mn}}\right)=\frac{F_0}{i\psi^*_{m'n'}}, \tag{3.9b}$$

where $m'=0,\ldots,M,\ n'=1,\ldots,N$. Equation (3.9b) is the complex conjugate of equation (3.9a). These two results represent a linear set of $2MN$ equations for the $2MN$ unknowns w_{mn} and w^*_{mn}.

All unknowns, real(w_0), Ψ_{mn} and w_{mn}, can now be determined from equations (3.7)–(3.9). These quantities fully describe the motion of the friction-driven wheel.

The equations can be solved numerically (see Section 4.2), or they can be simplified with certain assumptions and then solved analytically.

An analytical solution of equation (3.8) for the complex eigenfrequencies is of particular interest. This equation can be approximated to give an explicit expression for the growth rate Δ_{mn} of the friction-driven wheel. The following assumptions are made for the approximation:

$$\Omega_{mn} \approx \omega_{mn} \quad \text{(similar frequencies of friction-driven and free wheel)}, \tag{3.10a}$$

$$|\delta_{mn}| \ll \omega_{mn} \quad \text{(small growth rate of free wheel)}, \tag{3.10b}$$

$$|\Delta_{mn}| \ll \Omega_{mn} \quad \text{(small growth rate of friction-driven wheel)}. \tag{3.10c}$$

These assumptions are supported by experimental evidence. As a consequence, the denominator of the term $g_{m'n'}/(\Psi_{mn} - \psi_{m'n'})$ becomes very small for $(m', n') = (m, n)$, and thus this term dominates over all the others. The sum in equation (3.8) then reduces to a single term, giving

$$\tfrac{1}{2}\gamma\Psi_{mn}\frac{g_{mn}}{\Psi_{mn} - \psi_{mn}} \approx 1. \tag{3.11}$$

This can be converted into an explicit equation for Ψ_{mn}, and after taking into account that g_{mn} is purely imaginary, with imaginary part $g^{(i)}_{mn}$,

$$g_{mn} = \mathrm{i}g^{(i)}_{mn} \tag{3.12}$$

(this ensures that the Green's function is continuous at $t = t'$, see equation (2.3)), one obtains

$$\Psi_{mn} \approx \frac{\psi_{mn}}{1 - \tfrac{1}{2}\gamma\mathrm{i}g^{(i)}_{mn}}. \tag{3.13}$$

The quotient in equation (3.13) can be brought into the standard form of a complex number, and this can then be simplified by the further assumption that $\gamma^2(g^{(i)}_{mn})^2 \ll 1$.

Subsequent substitution for ψ_{mn} and Ψ_{mn} with equations (2.4) and (3.1), respectively, gives

$$\Omega_{mn} + \mathrm{i}\Delta_{mn} \approx (\omega_{mn} + \mathrm{i}\delta_{mn})(1 + \tfrac{1}{2}\gamma\mathrm{i}g^{(i)}_{mn}), \tag{3.14}$$

and comparison of the imaginary parts of equation (3.14) gives

$$\Delta_{mn} \approx \delta_{mn} + \tfrac{1}{2}\gamma\omega_{mn}g^{(i)}_{mn}. \tag{3.15}$$

Equation (3.15) gives the approximate growth rate of mode (m, n) of the friction-driven wheel. This is positive, indicating that mode (m, n) is unstable, if

$$\delta_{mn} + \tfrac{1}{2}\gamma\omega_{mn}g^{(i)}_{mn} > 0. \tag{3.16}$$

Inequality (3.16) is satisfied, if the term $\frac{1}{2}\gamma\omega_{mn}g^{(i)}_{mn}$ is positive and sufficiently large to counteract the growth rate δ_{mn}, which is negative and a measure of the damping of the free wheel. ω_{mn} is always positive; $g^{(i)}_{mn}$ is also positive, otherwise mode (m, n) of the Green's function would be displaced in the opposite, rather than the same, direction of the impulse force immediately after $t = t'$ (see equation (2.3a), with $g_{mn}(r_f, \varphi_f; r_f, \varphi_f) = \mathrm{i}g^{(i)}_{mn}$). The criterion (3.16) includes properties of the Green's function (ω_{mn}, δ_{mn}, $g^{(i)}_{mn}$) and a property of the friction characteristic (γ representing "negative damping", but not F_0 representing the mean friction force). The following features make mode (m, n) prone to instability: δ_{mn} close to zero, large $\omega_{mn}g^{(i)}_{mn}$, and large positive γ.

4. NUMERICAL RESULTS

4.1. PROPERTIES OF THE WHEEL AND PARAMETERS OF THE FRICTION CHARACTERISTIC

In our numerical simulations, we consider a small model wheel. It is made from steel with the following material properties; $\rho = 8000\ \mathrm{kg/m^3}$ (mass density), $E = 2 \times 10^{11}\ \mathrm{N/m^2}$ (Young's modulus), $\nu = 0{\cdot}3$ (Poisson ratio).

It is shaped like a flat circular disc with a hub at the centre and has the following measurements: $d = 0{\cdot}003$ m (wheel thickness), $a = 0{\cdot}038$ m (wheel radius), $b = 0{\cdot}01$ m (radius of wheel hub).

The wheel is excited by a friction force, which is described by the linear friction characteristic (2.2) and the following parameters: $\gamma = 15\,000$ N s/m (slope of the slip section), $F_0 = 1{\cdot}07$ N (mean friction force).

Only the first five modes ($m = 0, \ldots, 4$, $n = 1$) have eigenfrequencies within the range of audible frequencies, and only those modes are included in the numerical simulations presented here.

In the companion paper by Heckl and Abrahams [7], the same wheel was considered, and it was excited by the same (linear) friction force. The time history was calculated by solving the governing equation by an iteration in the time domain for various sets of modal loss factors. Here, we calculate the modal properties of the wheel in the frequency domain, for the same sets of modal loss factors, to allow a comparison of both methods.

4.2. EIGENFREQUENCIES, GROWTH RATES AND AMPLITUDES

The eigenfrequencies ω_{mn} of the free wheel and its Green's function amplitudes $g^{(i)}_{mn}$ are listed in Table 1. These values were kept constant in all simulations. The modal loss factors were varied, leading to different sets of growth rates δ_{mn}, which are listed in Tables 2(a)–(d). Also listed in these tables are the properties of the

TABLE 1

Properties of the free wheel

m	n	ω_{mn} $(2\pi\,\mathrm{s}^{-1})$	$g_{mn}^{(i)}$ $(10^{-9}\,\mathrm{m/N\,s})$
0	1	3020	1969
1	1	2922	4124
2	1	3655	3472
3	1	6482	2141
4	1	10980	1409

TABLE 2

For the free wheel: growth rates δ_{mn}; for the friction-driven wheel: growth rates Δ_{mn} (analytical estimate in parantheses), frequencies Ω_{mn}, and complex amplitudes w_{mn}

m	n	δ_{mn} (s^{-1})	Δ_{mn} (s^{-1})	Ω_{mn} $(2\pi\,\mathrm{s}^{-1})$	real w_{mn} $(10^{-10}\,\mathrm{m})$	imag w_{mn} $(10^{-10}\,\mathrm{m})$
(a)						
0	1	−1328	−1198(−1048)	2993	0·252	−0·189
1	1	−1285	−598(−717)	2975	−1·887	0·665
2	1	−161	474(437)	3637	−0·929	−0·282
3	1	−2851	−2200(−2197)	6480	−0·271	−0·057
4	1	−4829	−4103(−4101)	10979	−0·106	−0·022
(b)						
0	1	−1328	−1201(−1048)	2992	0·258	−0·171
1	1	−1285	−563(−717)	2977	−2·033	0·658
2	1	−1607	−1011(−1009)	3642	−0·773	−0·341
3	1	−163	496(491)	6473	−0·285	−0·041
4	1	−4829	−4105(−4101)	10979	−0·105	−0·022
(c)						
0	1	−1328	−1198(−1048)	2992	0·254	−0·186
1	1	−1285	−593(−717)	2976	−1·912	0·672
2	1	−459	167(139)	3638	−0·895	−0·300
3	1	−81	575(572)	6473	−0·284	−0·040
4	1	−4829	−4105(−4101)	10979	−0·105	−0·022
(d)						
0	1	−1328	−1198(−1048)	2993	0·252	−0·189
1	1	−1285	−599(−717)	2975	−1·884	0·665
2	1	−184	449(414)	3637	−0·923	−0·280
3	1	−244	411(410)	6473	−0·283	−0·041
4	1	−4829	−4105(−4101)	10979	−0·105	−0·221

friction-driven wheel. The frequencies Ω_{mn} and growth rates Δ_{mn} were calculated as the real and imaginary part of Ψ_{mn}, which are the roots of the non-linear equation (3.8). This equation was solved by the Newton/Raphson method (starting value for

the iteration: $\Omega_{mn} = \omega_{mn}$, Δ_{mn} from equation (3.15)). The estimated growth rates Δ_{mn}, using the analytical result (3.15), are listed in brackets. The linear set of equations (3.9a, b) gave the complex amplitudes w_{mn}.

The results listed in Tables 2(a)–(d) correspond to the time histories shown in Figures 7(a)–(d) respectively in reference [7]. Mode (2, 1) is unstable in Table 2(a); mode (3, 1) is unstable in Table 2(b); modes (2, 1) and (3, 1) are unstable, with mode (3, 1) dominating, in Table 2(c); modes (2, 1) and (3, 1) are about equally unstable in Table 2(d). These results for the stability behaviour agree with those in reference [7]. The agreement goes even further. The time histories for the wheel velocity shown in that paper in Figures 7(a)–(d) can be reproduced quite accurately from the frequency-domain results in this paper: evaluation of the modal superposition (3.4) with the values for Ψ_{mn} ($= \Omega_{mn} + \mathrm{i}\Delta_{mn}$) and w_{mn}, listed in Table 2(a)–(d), gives time histories which deviate by less than 5% from the earlier ones.

The analytical considerations in Section 3 are also confirmed. The free-wheel frequency values, ω_{mn}, in Table 1 are very similar to their equivalents, Ω_{mn}, in Tables 2(a)–(d) for the friction-driven wheel, thus confirming the assumption (3.10a). The accurate value for the growth rate Δ_{mn} is listed in Tables 2(a)–(d), together with the analytical estimate from equation (3.15) (given in brackets). There is good agreement between the accurate and the estimated values.

5. CONCLUSIONS

The following features make a wheel mode prone to squeal: δ_{mn} (growth rate of the free wheel, and measure of its damping) close to zero; ω_{mn} and $g^{(i)}_{mn}$ (frequency of the free wheel and Green's function amplitude) large; γ ("negative-damping" coefficient associated with the friction force) large.

The mean value of the friction force does not influence the stability behaviour. The frequencies of the friction-driven wheel differ very little from the free-wheel frequencies.

The frequency-domain results in this paper confirm and complement the time-domain results in an earlier companion paper [7]. Both approaches have advantages: the frequency-domain approach allows a more systematic study of the stability behaviour of individual modes; this is particularly valuable if more than one mode is unstable. However, only a linear slip-only (rather than stick/slip) friction force can be taken into account, to give a criterion as to whether a mode is squeal-prone (rather than squealing). This limitation does not arise with the time-domain approach. It is a relatively easy programming task to produce time histories of the wheel motion with this approach, but not so easy to make out the stability behaviour of individual modes.

It would be desirable to extend the present study of a non-linear analysis in the frequency domain, taking the full stick/slip friction force into account and any modal interactions caused by this. This would give a direct criterion as to whether a mode is squealing; it might be an extension of the criterion above, in terms of properties of the free wheel and properties of the (non-linear) friction force.

REFERENCES

1. P. J. Remington 1985 *Journal of Sound and Vibration* **116**, 339–353. Wheel/rail squeal and impact noise: What do we know? What don't we know? Where do we go from here?
2. U. Fingberg 1990 *Journal of Sound and Vibration* **143**, 365–377. A model of wheel-rail squealing noise.
3. H. von Stappenbeck 1954 *Zeitschrift VDI* **96**, 171–175. Das Kurvengeräusch der Straßenbahn-Möglichkeiten zu seiner Unterdrückung.
4. M. J. Rudd 1976 *Journal of Sound and Vibration* **46**, 381–394. Wheel/rail nose—Part II: wheel squeal.
5. E. Schneider, K. Popp and H. Irretier 1988 *Journal of Sound and Vibration* **120**, 227–244. Noise generation in railway wheels due to rail-wheel contact forces.
6. F. Périard 1998 *Ph.D. Dissertation*, *Technische Universiteit Delft*: *ISBN* 90-9011964-7, *NUGI* 834. Wheel-rail noise generation: Curve squealing by trams.
7. Maria A. Heckl and I. D. Abrahams *Journal of Sound and Vibration*. Curve squeal of train wheels, Part 1: Mathematical model for its generation (submitted).
8. A. J. Jerri 1985 *Introduction to Integral Equations with Applications*. New York: Marcel Dekker Inc.
9. P. M. Morse and H. Feshbach 1953 *Methods of Theoretical Physics*, Part 1. New York: McGraw-Hill Publishing Company.